Quantitative characterization of ErbB receptor signaling platforms and their role in cancer

FINAL REPORT

Biophysical characterization of the homoclustering of ErbB3

Since we have successfully used number and brightness (N&B) analysis previously for the investigation of the clustering of ErbB1 and ErbB2, we started to use this method for ErbB3 proteins as well. Although our preliminary results revealed ErbB3 homoclusters in cells transfected with ErbB3-mYFP, we could not reproduce these initial results and we could not detect any changes in the clustering of ErbB3 upon stimulation with its ligand, heregulin (HRG). We considered two possibilities for the failure: (i) inappropriate photophysical properties of mYFP for single molecule studies. Therefore, we have recloned ErbB3 to a GFP vector. (ii) Methodological problems related to N&B analysis. Therefore, a collaboration was established with Gerhard Schütz (Technical University, Vienna) to investigate the problem with TOCCSL (Thinning out clusters while conserving stoichiometry of labeling). It these experiments it was found out that detection of signal from ErbB3 located in intracellular vesicles could also have led to problems in these kinds of experiments. Therefore, ErbB3 was labeled with AlexaFluor647-tagged anti-ErbB3 Fabs which label only membrane-exposed ErbB3. Using this strategy we found that ~5% of ErbB3 forms constitutive, ligand-independent dimers both in the absence and presence of ErbB2 coexpression. The lateral mobility of ErbB3 was 0.08 μm^2/sec in the absence of stimulation. HRG increased the fraction of ErbB3 dimers to ~16% accompanied by a reduction of the lateral mobility of the receptor to 0.04 μm^2/sec. Coexpression of ErbB2 slightly reduced the increase in the fraction of ErbB3 dimers after HRG stimulation.

Effect of the dipole potential on the clustering and signaling of ErbB proteins

The dipole potential is a strong electric field in the plasma membrane whose magnitude exceeds that of the transmembrane potential. Despite this fact, its effect on the clustering and functioning of membrane proteins has not been investigated. Using fluorescence ratiometric measurement of the dipole potential we confirmed that phloretin and 6-ketocholestanol decrease and increase, respectively, the dipole potential. An elevated dipole potential significantly reduced the binding of EGF without altering the expression level of the receptor (Fig. 1A). We investigated the homo- and heteroclustering of ErbB1 and ErbB2 using FRET and

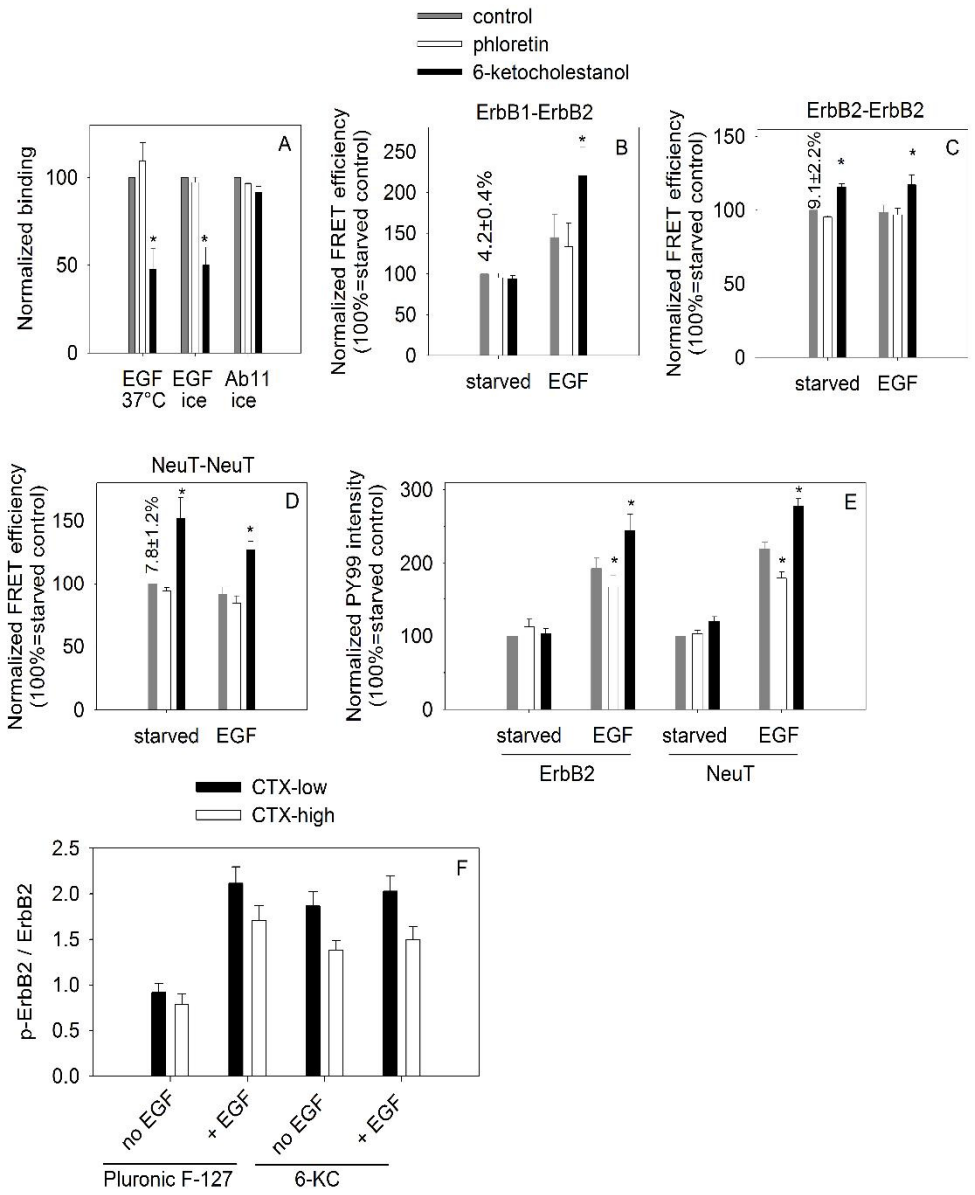

Figure 1. The effect of the dipole potential on ErbB proteins. The dipole potential was decreased and increased by phloretin and 6-ketocholestanol (6-KC), respectively. Since treatment of cells with both agents was carried out in the presence of Pluronic F-127, control samples were treated with this detergent. (A) EGF binding was significantly reduced at an elevated dipole potential, whereas expression of ErbB1 (EGF receptor), labeled by Ab11 antibody, was not influenced. (B-D) The heteroassociation of ErbB1 with ErbB2 (B), the homoclustering of ErbB2 (C) and NeuT (D) were measured flow cytometric FRET measurements. The measured values were normalized to the untreated control samples. Cells were serum-starved overnight followed by EGF stimulation. The numbers above the bars corresponding to the starved control samples represent the unnormalized FRET efficiency. (E) Flow cytometric determination of the tyrosine phosphorylation response of HeLa cells transfected with wild-type ErbB2 or NeuT. Phosphorylated tyrosine was labeled by the PY99 antibody. Values are normalized to the starved control. (F) Cells were stimulated with EGF as described above. Raft and non-raft regions were discriminated by labeling cells with subunit B of cholera toxin (CTX) with CTX-high regions corresponding to lipid rafts. Tyrosine phosphorylation of ErbB2 was determined by a phospho-specific anti-ErbB2 antibody (Ab18) and its intensity was normalized to ErbB2 expression. Asterisks indicate a significant ($p<0.05$) difference compared to the control of the respective group.

N&B measurements. Although the clustering of ErbB1 and ErbB2 were not sensitive to alterations in the dipole potential in resting cells, the ligand-induced formation of both their homo- and heteroclusters was significantly enhanced at an elevated dipole potential (Fig. 1BC). NeuT is a transmembrane domain mutant of ErbB2 which is activated even in the absence of ligand stimulation and it has been shown to transform cells. The effect of the dipole potential was stronger on NeuT than on wild-type ErbB2 (Fig. 1D). Increasing the dipole potential enhanced EGF-induced tyrosine phosphorylation of ErbB1 and ErbB2 (Fig. 1E). Since the dipole potential is assumed to be different in lipid rafts than in the rest of the membrane, we compared the EGF-induced tyrosine phosphorylation response in raft and non-raft domains at normal and elevated dipole potentials. EGF induced a larger increase in ErbB2 tyrosine phosphorylation outside lipid rafts and increasing the dipole potential had a stronger effect on ErbB2 tyrosine phosphorylation outside raft regions (Fig. 1F).

The influence of three-dimensional culture conditions and coculturing of mesenchymal stem cells on ErbB proteins

We established 3D culture conditions for SKBR-3 cells and analyzed the homoassociation of ErbB2 and the efficiency of transmembrane signaling in cells cultured under normal conditions and in 3D cell cultures. In order to label membrane proteins of cells in 3D cultures with fluorescent monoclonal antibodies frozen sections were cut with a cryostat. Microscopic fluorescence resonance energy transfer (FRET) measurements showed that ErbB2 was homoassociated in 3D cultures, whereas no or very low homoassociation tendency was observed in 2D cultures. We also compared the level of phosphorylation of ErbB1, ErbB2, MAPK and Akt in cells kept under the two different culturing conditions. ErbB1 and Akt were significantly less phosphorylated in 3D cultures (Fig. 2). Similar effects were detected regarding the signaling cascades when breast cancer cells were cultured in the presence of media conditioned with mesenchymal stem cells.

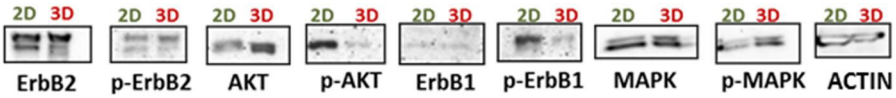

Figure 2. Analysis of activation and expression of proteins in cells cultured in 3D and conventional 2D cultures. SKBR-3 cells were cultured in 3D cultures for seven days and the expression and activation level of ErbB1, ErbB2, Akt and MAPK were compared in the two culture types using Western blotting.

Investigation of the chaotic behavior or ErbB1

In order to analyze the scale-free, power-law dependence of EGF-induced tyrosine phosphorylation A431 cells were transfected with a CFP-YFP tyrosine phosphorylation sensor in which the linker between the two fluorescent proteins contained an ErbB1 tyrosine phosphorylation site which undergoes a conformational change upon phosphorylation (PICCHU). The response to EGF was characterized by the difference in the FRET values before and after EGF stimulation on a cell-by-cell basis. The distribution of responses could not be fitted well with a power law. The experiments were repeated with CHO cells stably transfected with ErbB1-GFP. Due to the spectral crosstalk between the tyrosine phosphorylation sensor and GFP the EGF-induced response was characterized by staining cells with an anti-pTyr antibody after fixation and permeabilization. Based on the GFP fluorescence intensity proportional to EGF receptor expression cells were classified into low, medium and high expressers and their EGF-induced response was analyzed separately. While the response of cells expressing high numbers of EGF receptor could not be fitted with a power law, that of low expressers could be reasonably well approximated with a power law suggesting non-deterministic behavior. Since the curves were rather noisy, the experiments will have to be repeated in order to confirm these results.

Correlation between the efficiency of elisidepsin, the lipid composition of the cell membrane and hypoxia

Elisidepsin is an experimental chemotherapeutic drug whose mechanism of action was unknown at the time our investigations were initiated. Previously we and our Spanish collaborators showed that elisidepsin permeabilizes the plasma membrane. Another publication implicated FA2H (fatty acid 2-hydoxylase) as a marker enzyme for elisidepsin sensitivity. We confirmed that the sensitivity of cells to the drug indeed correlates with the expression level of FA2H (Fig. 3A). Since the mono-oxidation reaction catalyzed by FA2H requires oxygen, we argued that the drug must be less efficient under hypoxic conditions. After testing seven cell lines we concluded that cells with the highest level of FA2H expression were equally sensitive to the drug under normoxic and hypoxic conditions, whereas those with lower expression levels showed reduces sensitivity under hypoxic conditions (Fig. 3B). Using mass spectrometry we showed that the reduced level of hydroxylated fatty acids correlated with the reduction of sensitivity to elisidepsin. Replenishment of 2-OH palmitic acid restored

the diminished elisidepsin sensitivity of hypoxic cells implying that it was the reduction of hydroxylated fatty acid levels which led to the reduced elisidepsin sensitivity. Using a fluorescent elisidepsin analog we established that elisidepsin binding in inhibited under hypoxic conditions in those cells whose sensitivity was oxygen-dependent (Fig. 3C). Although the concentration dependence of elisidepsin binding did not show cooperativity, membrane permeabilization and consequent cell killing showed very strong cooperativity (Fig. 3D). We generated a model in which a threshold concentration of elisidepsin required for killing was assumed. This model could successfully reproduce the lack of cooperativity in binding and the apparent high cooperativity in the killing curve. The binding of fluorescent elisidepsin showed a strong positive correlation with lipid rafts in accordance with the preferential localization of hydroxylated lipids in rafts (Fig. 3E). Our results explain the lack of efficiency of elisidepsin in clinical trials in which the drug was tested in patients with advanced cancer in which hypoxia is wide-spread.

Relationship between the effectivity of epigallocatechin-gallate (EGCG) and lipid rafts

After establishing the relationship between the effect of elisidepsin and lipid rafts, we tested other compounds whose mechanism of action may be linked to lipid rafts. Two natural compounds, EGCG and genistein, were shown to have anti-proliferative effects on SKBR-3 and A431 cells. While EGCG was more efficient in inducing cell death, genistein blocked cell cycle progression in the G2/M phase (Fig. 4AB). 67LR (67 kDa laminin receptor) is a non-integrin laminin receptor. Antibodies against 67LR inhibited the anti-proliferative effect of EGCG in A431, but not in SKBR-3 cells implying that 67LR is involved in the mechanism of action of the compound, at least in some cell lines. EGCG induced a ~40-50% downregulation of ErbB1 and ErbB2 expression, while genistein did not modify the expression of these receptors. 67LR showed strong colocalization with lipid rafts in untreated cells, while its lipid raft localization was partially abolished by treatment with EGCG (Fig. 4C). These results implied that lipid rafts may have something to do with the mechanism of action of EGCG. This assumption was corroborated by N&B analysis showing that the homoclustering of GFP-GPI, a lipid raft marker, was diminished by EGCG. We concluded that the primary target of EGCG may be the lipid raft component of the plasma membrane followed by secondary changes in the expression of ErbB proteins, while genistein must have other unidentified targets.

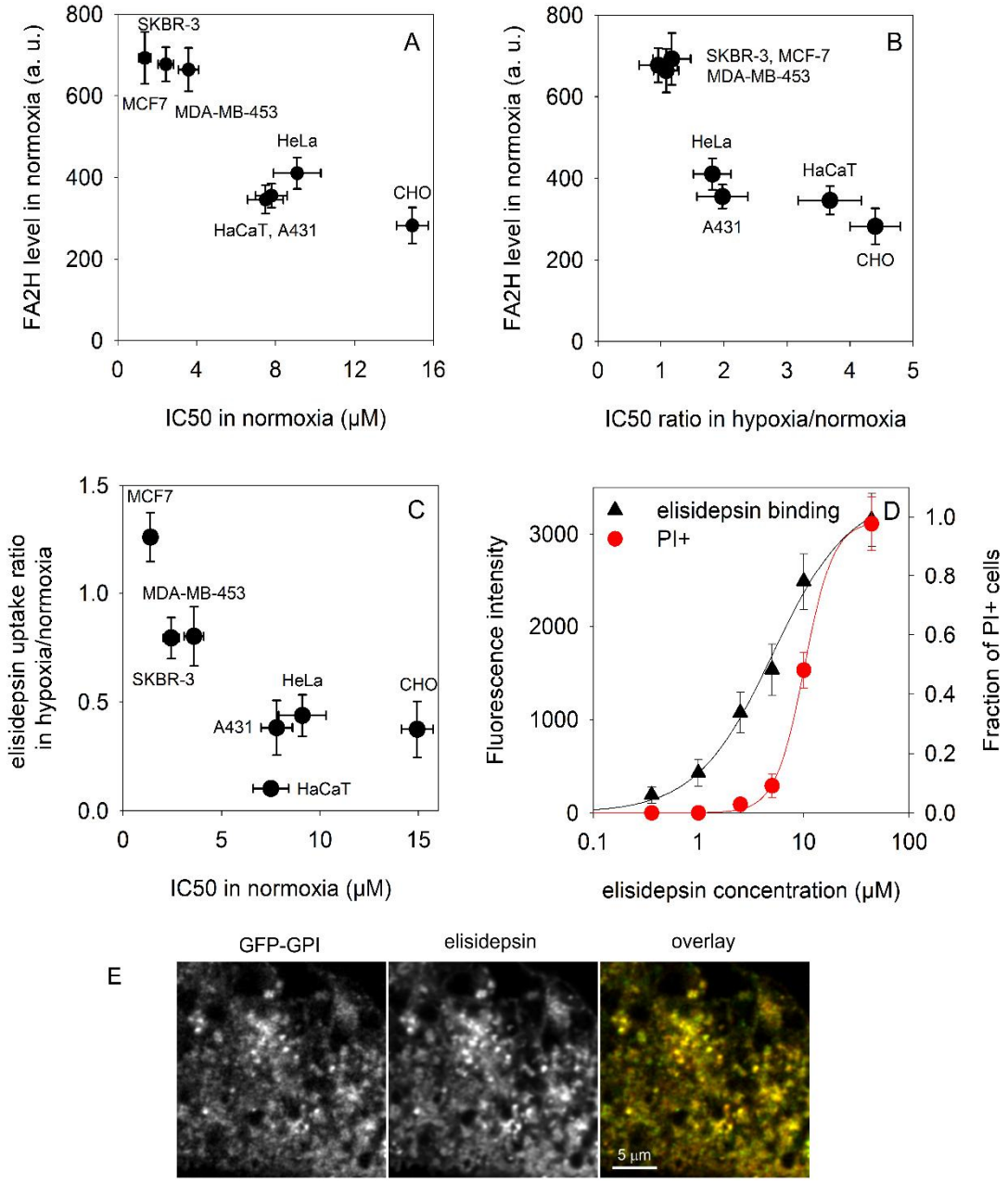

Figure 3. Hypoxia-induced alterations in elisidepsin sensitivity. (A-B) The FA2H level, determined by immunofluorescence, is plotted against the half-maximal inhibitory concentration of elisidepsin (IC50) in normoxia (A) and against the fold-change in the IC50 induced by hypoxic culture conditions (B). (C) The binding of elisidepsin to the membrane was determined using a fluorescent elisidepsin analog and its intensity was plotted as a function of the IC50 of elisidepsin in normoxia. (D) The concentration dependence of binding of elisidepsin to the membrane and the dose dependence of the elisidepsin-induced cell killing determined as the fraction of propidium iodide (PI) positive cells are shown. (E) Cells transfected with GFP-GPI (glycosyl-phosphatidylinositol-anchored GFP) and treated with fluorescent elisidepsin. Green and red correspond to GFP-GPI and elisidepsin, respectively, in the color overlay.

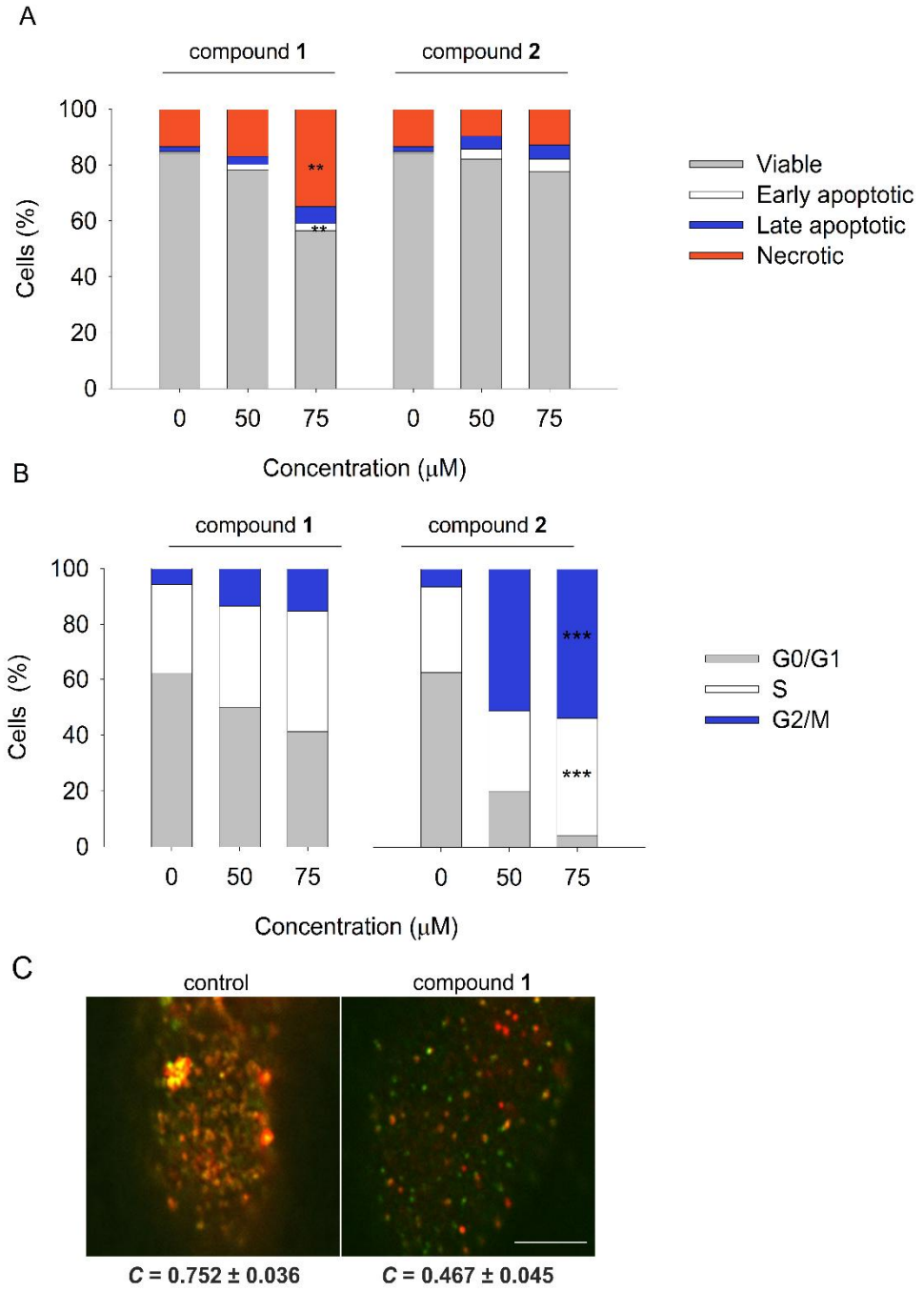

Figure 4. Investigation of the effect of EGCG and genistein. (A-B) SKBR-3 breast cancer cells were treated with the indicated concentrations of EGCG (compound 1) and genistein (compound 2) for 72 h followed by staining with annexin V-FITC and 7-AAD for flow cytometric measurement of apoptosis and necrosis (A). Alternatively, cells were stained with propidium iodide for cell cycle analysis (B). (C) A431 cells were incubated with EGCG for 30 min at 37 °C followed by staining with fluorescent subunit B of cholera toxin (red) and with a monoclonal antibody against 67LR (green). *C* stands for the Pearson correlation coefficient. The asterisks indicate a significant difference compared to the control (**p < 0.01, ***p < 0.001).

Development of novel FRET-evaluation algorithms

Our group has been using microscopic FRET measurements for studying the interaction of membrane proteins. In many cases we faced significant problems when the signal-to-noise ratio was low resulting in noise-dominated FRET histograms or FRET images. We developed a novel way to estimate the FRET efficiency in intensity-based FRET calculations based on the Poisson statistics of photon detection. It was assumed that a single FRET efficiency characterizes all pixels in the image. Intensities measured in the donor, FRET and acceptor channels were assumed to be contaminated by Poissonian noise. The likelihood of the measured intensities with the FRET efficiency as an unknown parameter was expressed and maximum likelihood estimation was carried out to determine the FRET efficiency maximizing the likelihood for all pixels. Testing the algorithm with simulated datasets showed that it can estimate the FRET efficiency accurately with as low as five detected photons/pixel (number of

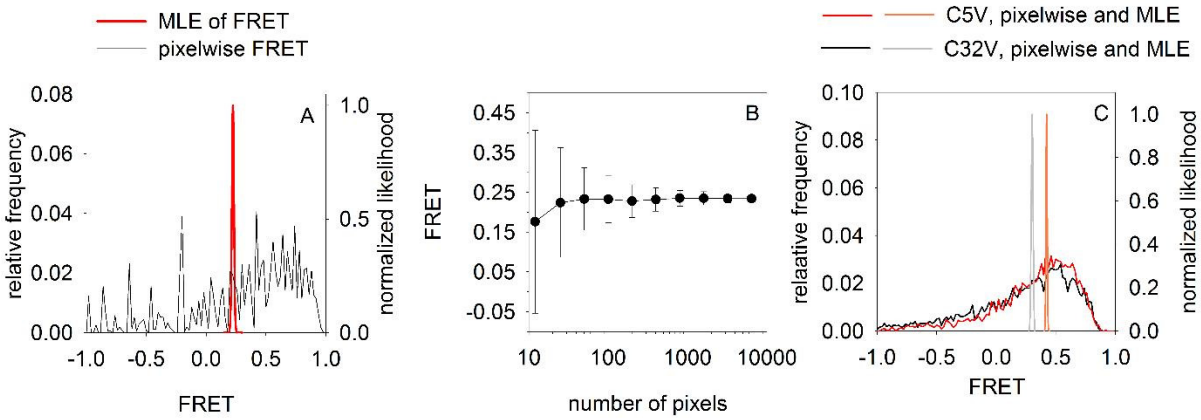

Figure 5. Maximum likelihood estimation of FRET efficiency. (A) Datasets containing 5000 pixels were generated in which the mean photon number/pixel was five and the FRET efficiency was 0.25. FRET was calculated for every individual pixel (black). The red histogram shows the confidence plot of the FRET efficiency determined by maximum likelihood estimation. (B) Random datasets containing different numbers of pixels were generated assuming a mean photon number of 10/pixel and a FRET efficiency of 0.25. The simulation was carried out 100-times and the mean±SD of the FRET values determined by maximum likelihood estimation as a function of the size of the dataset was plotted. (C) Cells were transfected with a construct in which Cerulean and Venus were separated by a 5-amino acid (C5V) or a 32-amino acid linker (C32V). Images were captured in the donor, FRET and acceptor channels using a confocal microscope operating in the photon counting mode. FRET was determined on a pixel-by-pixel basis and the distribution of FRET values is displayed by the red and black lines. FRET was also calculated by maximum likelihood estimation and the confidence interval of the determined FRET value is shown by the orange and gray lines.

pixels=5000, Fig. 5A). We tested how many pixels are required for the algorithm to work reliably. The simulations showed that 50-100 pixels are required for accurate estimations if the mean photon number is 10/pixel (Fig. 5B). The approach was also tested with experimental data. Cells were transfected with different FRET calibration constructs composed of Cerulean and Venus fluorescent proteins separated by linkers of different lengths. Maximum likelihood estimation of the FRET efficiency worked reliably at such low intensities when pixelwise calculations performed poorly (Fig. 5C). The algorithms were initially implemented in Mathematica, but later a user-friendly graphical user interface-controlled Matlab application was developed for performing intensity-based pixelwise calculations and maximum likelihood estimation of FRET efficiency.

Implementation of a new algorithm for the evaluation of colocalization between lipid rafts and membrane proteins

Quantitative evaluation of colocalization between fluorescently labeled proteins is complicated due to the lack of information about the confidence interval of the correlation coefficient obtained for a pair of labels without colocalization. We have implemented the method of Costes in Matlab and applied it for evaluating the colocalization between lipid rafts, IL-2 and IL-9 receptor alpha subunits. Thanks to the quantitative evaluation carried out on individual cells we have revealed that the distribution of the alpha subunit of IL-9 receptors (IL-9R) displays a bipartite nature in that it either shows strong colocalization with or segregation from lipid rafts. Lipid rafts were defined by labeling with fluorescent cholera toxin and these membrane domains showed strong colocalization with MHC-I and IL-2R-containing membrane areas. The bipartite behavior of IL-9 receptor was mirrored by STAT phosphorylation also revealing two populations of cells in which IL-9 receptors show colocalization with and segregation from lipid rafts.